Electrochimica Acta 191 (2016) 521–529

Contents lists available at ScienceDirect

Electrochimica Acta

journal homepage: www.elsevier.com/locate/electacta

Understanding the effect of morphology on the photocatalytic activity of TiO_2 nanotube array electrodes

C. Adán, J. Marugán*, E. Sánchez, C. Pablos, R. van Grieken

Department of Chemical and Environmental Technology (ESCET), Universidad Rey Juan Carlos, C/Tulipán s/n, 28933 Móstoles (Madrid), Spain

ARTICLE INFO

Article history:
Received 6 November 2015
Received in revised form 23 December 2015
Accepted 12 January 2016
Available online 15 January 2016

Keywords:
TiO_2 nanotubes
Morphology
Photocurrent
Photocatalysis
Photoelectrocatalysis

ABSTRACT

A comprehensive report on the correlation between the morphology and the photocatalytic (PC) and photoelectrocatalytic (PEC) activity of TiO_2 nanotubes (NTs) electrodes is presented. New insights are provided to support the effect of the anodization conditions on the photon-to-current efficiency of the electrodes based on the dimensional characteristics of the TiO_2-NTs. Electrodes with promising properties based on the characterization data were scaled-up to test their activity on the PC and PEC oxidation of methanol. Results indicate that the length of the nanotubes significantly influences the photodegradation efficiency. The enhancement achieved in both PC and PEC processes with longer nanotubes can be explained by the higher surface area in contact with the electrolyte and the increase in the light absorption as the TiO_2 layer becomes thicker. However, as the length of the nanotubes increases, a reduction in the enhancement achieved by the application of a potential bias is observed. Kinetic constants of both reactions (PC and PEC) tend to get closer and the charge separation effect diminishes. In relative terms, the effect of the electric potential is more pronounced for electrodes with the shorter NTs. The reason is that once the TiO_2 layer is thick enough to absorb the available radiation, a further increase in the NTs length increases the resistance of the electrons to reach the back contact and the diffusional restrictions to the mass transport of the reactants/products along the tubes. Consequently, the existence of a compromise between reactivity and transport properties lead to the existence of an optimal NTs length.

1. INTRODUCTION

Titanium dioxide (TiO_2) nanotubes (NTs) with different structures and morphologies have drawn much attention in the last years. In particular, several applications for highly ordered nanostructures of TiO_2, as nanotubes or nanowires have emerged [1,2]. The main reason is that TiO_2 nanotubes display an increased surface-area-to-volume ratio compare with particulate TiO_2 structures. Furthermore, the electron transport velocity and charge separation efficiency also increase, reducing charge recombination rate and making these materials ideal for solar or UV light photoelectronics applications. These characteristics make them attractive for a wide range of applications in many technological fields, as hydrogen generation [3], battery electrodes [4], sensors [5], solar cells [6,7] and photocatalytic and photoelectrocatalytic applications [8,9], being one of the most intensively studied nanomaterials.

A number of techniques have been used to prepare TiO_2 NTs configurations, such as hydrothermal treatment of TiO_2 in NaOH solution, anodization of titanium sheets, template methods, and electrospinning [1,2,8,10,11]. The most common procedures are based on the hydrothermal method [1,12] and the electrochemical anodic oxidation [2,13]. Hydrothermal synthesis starts when a TiO_2 precursor is dissolved in a concentrated aqueous solution of NaOH. The obtained mixture is placed into an autoclave and converted into a crystalline tubular nanostructure at 110–150 °C. The final material needs to be washed with diluted acidic aqueous solution or solvents [1,10]. On the other hand, the electrochemical anodic oxidation method is completely different and can be easily carried out by the field assisted oxidation of Ti metal to form titanium dioxide in an electrolyte that generally is constituted by a fluoride salt, water and an organic polar compound as main liquid phase [2,14]. The formation of the NTs geometry starts with the application of an anodic voltage to the metallic titanium foil to produce a stable compact TiO_2 layer due to the electrochemical oxidation of titanium. After that, fluoride ions present in the electrolyte are responsible for the formation of NTs by the field assisted dissolution of Ti metal to form titanium dioxide and the

* Corresponding author. Tel.: +34 91 664 7466; fax: +34 91 488 7068.
E-mail address: javier.marugan@urjc.es (J. Marugán).

http://dx.doi.org/10.1016/j.electacta.2016.01.088
0013-4686/

chemical dissolution of Ti and TiO_2 due to etching by these ions [14,15].

Although both methods seem to be very simple, every single synthesis step plays a crucial role in controlling the final properties of the NTs. This is one of the reasons of the great number of articles focusing on the preparation of self-organized TiO_2 nanotubular structures with a large potential to enhance novel functional features. Other important features of TiO_2 NTs are the remarkable rapid and long-distance electron-transport capability [16] and the enhancement in the light absorption due to the high ratio of length to pore diameter [17], both of which will improve photocatalytic efficiency [8,18].

Therefore, many authors have focused their studies on the preparation conditions and have determined the influence of many synthesis variables. In the case of the anodization of Ti foils, the applied anodization potential or current density and the anodization time are one of the most important, influential and studied parameters [14,18–24]. Other variables are related to the composition of the electrolyte employed such as the concentration of water or fluor salt [2], the polar organic electrolyte employed [2,25], or the acidification of the electrolyte [2,14,25–27] or other factors like the temperature treatment [2,28], or pulsed anodic oxidation [29], among others. Most of these variables, significantly affect the geometrical parameters [18,22,24,28,30], the physico-chemical properties [2,14], the photocurrent response [25] and therefore the photocatalytic and electrophotocatalytic activity of the NTs [11,24,31]. Therefore, it is important to note that to obtain the desired characteristics of the nanotubes the preparation conditions must be optimized previously.

Additionally, the fact that these TiO_2-NTs arrays can be immobilized onto an electrically conducting support make them very attractive to be used as photoelectrodes for solar energy conversion and/or in electrolytic cells (i.e. photogeneration of useful products such as hydrogen, degradation of organic pollutants or reduction of CO_2) [32]. The reason is that these photoanodes offer the possibility of enhancing the photocatalytic activity of the TiO_2 layer by applying a positive bias potential. The electrical field provides a convenient way for transferring photogenerated electrons to the conductive substrate and be effectively extracted to the outer circuit, which results in an improved separation of photogenerated electron-hole pairs and better use of the photogenerated holes [8,16–18]. The main advantage of photoelectrocatalytitic processes over pure photocatalytic reactions is that the application of a potential bias reduces the electron-hole recombination, resulting in higher quantum efficiencies. In TiO_2 electrodes the photoelectrocatalytic activity can be related to the photocurrent density shown under the same operational conditions. However, in some cases this correlation is not linear due to multitude processes involved in phenomena of absorption and charge transfer [33]. For example, TiO_2 particulate films have been widely reported in the literature for photoelectrocatalytic applications [24,33–35]. These films are composed of interconnected TiO_2 nanoparticles and show a porous surface and a quite large surface area. However, that kind of film suffers from structural disorders and vast grain boundaries, which bring obstacles to the electron transport and affect the charge separation efficiency while the ordered nanotube architecture can provide a unidirectional electric channel for the transport of the photogenerated electrons [24]. This work focuses on the understanding of the correlation between the morphology and photocatalytic activity of TiO_2-NTs electrodes based on the analysis of the photocurrent densities and the incident photon-to-current efficiencies. It constitutes a novel comprehensive study of the influence of the morphological features of ordered titanium dioxide nanotube arrays to optimize the compromise between radiation absorption, surface area and electron and mass transport that maximizes the global reaction rate.

2. MATERIALS AND METHODS

Commercial titanium sheets (1 mm thick, 99.6% purity) of 1 cm (for physico-chemical characterization) and 5 cm in diameter (scaled-up for activity experiments) were supplied by Goodfellow Inc. A titanium wire was spot-welded to each of the sheets for the electrical connection during the anodization process and photoelectrocatalytic reactions. Before anodization takes place, all the sheets were degreased through sonication in ethanol for 15 minutes, and rinsing with deionized water. Then the foils were immersed again during two minutes in a $HF/HNO_3/H_2O$ (1:4:5 v/v) solution, and rinsed again in abundant deionized water.

The anodization process was conducted in a two-electrode electrochemical cell connected to a DC power supply (ISO-TECH, model IPS 303DD). A nickel mesh (Goodfellow Inc., 55% open area) was used as the cathode at a distance of 1 cm from the titanium anode. Subsequently the electrolytic solution is added to the electrochemical cell and then the selected anodization potential is applied without magnetic stirring. Two series of five electrodes were anodized with an electrolyte composed by ethylene glycol, water 5 wt% and NH_4F (0.15 M). The first set of electrodes was anodized keeping the applied potential constant at 20 V and modifying anodizing times at 60, 90, 120, 150 and 180 minutes. The second set of electrodes was anodized fixing the anodization time at 120 minutes, and variable potential of 10, 15, 20, 25 and 30 V. When the anodization process is finished the titanium foils are dried at 100 °C for 24 hours. After that time the electrodes are annealed at 450 °C during two hours with a heating ramp of 2 °C/min to induce anatase crystalline phase formation.

The crystal structure of the TiO_2-NTs electrodes was identified with an X-ray diffractometer (Philips X'Pert-MPD, Cu Kα radiation, equipped with an XCell detector). Each diffractogram was performed with scanning speed of 0.01/s and with an accumulation time of 2 s per point. Crystal particle size was calculated applying the Scherrer's equation.

Raman spectra of the TiO_2-NTs were obtained with a HORIBA Jovin-Yvon spectrometer model HR800UV equipped with an Olympus BX41 optic microscope. TiO_2-NT electrodes were excited with a red laser of 632.8 nm and spectra were registered between 100 y 800 cm^{-1}.

Diffuse reflection spectra (DRS) were recorded on a UV-visible spectrometer (Varian Cary 500 Scan UV-VIS-NIR) in the 250–450 nm regions using a Ti foil to register the base line. Band-gap values were determine by the optical absorption near the band edge by the equation $\alpha h\upsilon = A(h\upsilon - E_g)^{n/2}$ [36]. where α is the absorption coefficient, h is the Planck constant, υ is the radiation frequency, E_g is the band gap, A is a constant and n value is 4 for the direct transitions in the semiconductor.

The morphology, length, diameter and wall thickness of the nanotubular titanium dioxide films were evaluated using a high resolution Scanning Electron Microscopy (SEM). The images were realized with a Nova Nano SEM230 (FEG-SEM) microscope working with acceleration voltages between 2 y 10 kV and equipped with ETD, TLD, BSD, Helix, and CD detectors. Samples were previously prepared by scratching the intact surface and rotating the sample holder 45° to obtain the length of the TiO_2 nanotubes. The *Digital Micrograph 365 Demo* program from Gatan Sofware Company was used to analyze SEM images. The average pore diameter was calculated from 5 different FEG-SEM top-view images and standard deviation of the measurements were taken at less 10 measures of each parameter. The estimation of the porosity of the electrodes has been done following the methodology proposed by Kontos et al [37].

Determination of photocurrent densities by cyclic voltammetry were carried out using a cylindrical electrochemical cell in a three electrodes configuration. The anodized TiO_2-NTs electrode has been used as the photoanode, and a nickel mesh and Ag/AgCl (saturated in 3.0 M KCl) acted as the counter and reference electrodes, respectively. The photoanode was placed perpendicular to four UV lamps (Philips TL 6W), with an emission range between 340–400 nm (maximum at 365 nm) and an incident photon flow of 0.70 W m^{-2}. Measurements were recorder at scan sweep of 0.5 mV/s between 0 and 1.4 V for 4 cycles with a potentiostat Eco-Chemie μAUTOLAB Type III. The electrolyte consists of a 0.1 M Na_2SO_4 + 1 M CH_3OH aqueous solution. The recorded photocurrent values were transformed into photocurrent densities by considering the irradiated or photoactive surface of the electrodes (0.79 cm^2 or 19.64 cm^2, depending on the electrode size).

Determination of the photocatalytic (PC) and photoelectrocatalytic (PEC) activities of the electrodes was carried out using 5 cm diameter electrodes and methanol oxidation as model reaction. Methanol was transformed into formaldehyde during one-hour experiments of PC and PEC degradation at initial concentrations of 0.01, 0.1 and 1 M, using 0.1 M Na_2SO_4 as electrolyte. In the PC experiments the electrodes were placed in the cell without connection to the power supply while for the PEC experiments a potential bias of 1 V was applied between the working and the counter electrode. The formaldehyde evolution of the reaction was followed through the colorimetric determination of the formaldehyde at 412 nm produced along the reaction following the Nash's method [38]. Absorbance was measured with a Biochrom Libra S22 spectrophotometer with an optical path of 1 cm.

3. RESULTS AND DISCUSSION

3.1. Physicochemical and morphological characterization

Main physico-chemical characterization results are shown in the supplementary data. X-ray diffraction patterns (see Fig. 1S) have shown the formation of the crystalline anatase phase, with no signs of rutile in both series of TiO_2-NTs electrodes. The anatase peak intensity gradually increases as anodization potential and time increase, although this effect is more evident for the variation of anodization potential. The anatase crystallite size, calculated from the more intense 101 diffraction signal at 25.3°, was around 32–39 nm in all the electrodes (see Table 1S), in agreement with previous reports [2]. Raman spectra from both series of electrodes (showed in Fig. 2S) also verified the existence of the well-crystallized anatase phase in the photoanodes. Raman bands intensities increase for higher anodization potential and time, in agreement with the higher degree of crystallization observed by X-Ray diffraction. Raman spectra also confirm a more significant effect of the change in anodization potential in comparison with the effect of the anodization time. Higher intensities of the Raman bands have been related to an increase in the thickness of the TiO_2 layer and therefore, an increase in the length of the TiO_2-NTs [17]. This supposition has been confirmed by the measurement of the TiO_2-NTs dimensions by Electron Scanning Microscopy.

Fig. 1 shows the dependence of the NTs length versus anodization potential and time for both series of electrodes. The micrographs added to the figure reveal well defined porous structures in all the photoanodes. As it was expected, the length of these self-organized structures linearly increases with applied voltage and anodization time, although the effect was more pronounced for the variation of the potential bias. As the potential increases, the resulting nanotube length was found to exhibit a strong dependence on the applied voltage, from 10 to 30 V, as confirmed by other authors [14]. According to these results, nanotube length increases linearly at approximately 111 nm V^{-1}

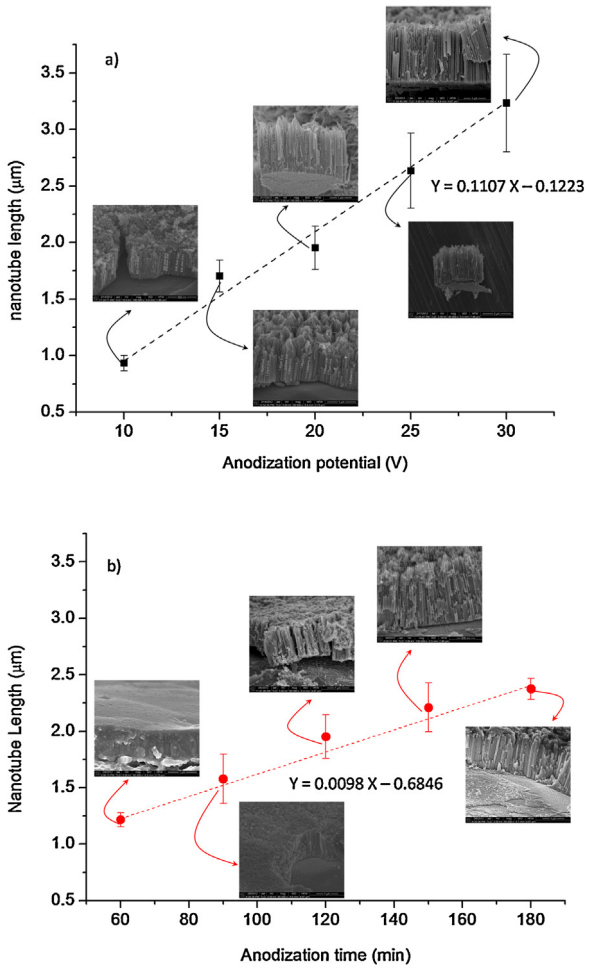

Fig. 1. Influence on the average length of the TiO_2-NTs of the a) variation of anodization potential at 120 min of anodization time, and b) variation of anodization time at 20 V of anodization potential. Inset: Representative SEM images of cross-sections of the electrodes.

between 10 and 30 V. The reason is that during the nanotube growth step, a thin and compact TiO_2 barrier layer at the pore bottom/electrolyte interface is continuously dissolved by increased field, and a new barrier layer at the metal/oxide interface (Ti/TiO_2) is rebuilt [14]. Thus when anodization voltage increases also the driving force for ionic transport through the barrier layer at the bottom of the pore increases and the movement of the Ti/TiO_2 interface into the titanium metal surface is faster. This fact results in a higher assisted oxidation of Ti metal to form titanium dioxide [22,25]. Our results show that the maximum tube length achieved in this set of electrodes was 3.23 ± 0.43 μm that corresponds to a titanium foil anodized at 30 V during 120 minutes. The application of different anodization times also had a critical role in deciding the uniformity of nanostructure formation. The variation of anodization time results in a speed of growth of NTs of 9.8 nm min^{-1} when time increases from 60 to 180 minutes, eleven times smaller than that observed in the set of electrodes by anodizing potential variation.

On the other hand, the variation of inner and outer tube diameter and wall thickness versus anodization potential and time is showed in supplementary data (Fig. 3S). Although an increase in anodizing potential gives rise to an increase in the inner and outer pore diameters, the nanotubes diameters and wall thicknesses are independent of the anodization time and remain almost constant in the studied range, as shown in Fig. 3Sb.

For more information, Table 1S summarizes the physicochemical properties and estimated morphological parameters of the photoelectrodes. The band gap values of the electrodes calculated by the edge extrapolation are also collected in Table 1.S, ranging from 3.44 to 3.33 eV. As expected for nanocrystallites, these values are higher than that of 3.2 corresponding to well crystallized anatase monocrystals. A slightly decrease in *Eg* is observed as the NTs grow longer for higher anodization voltage and time, shifting the UV photoresponse towards the visible-light spectrum.

3.2. Photoelectrochemical characterization

Fig. 2 shows the photocurrent density (I_{ph}) –electric potential (E) curves of the TiO_2-NTs electrodes under UV-A illumination in 0.1 M $NaSO_4$ and 0.1 M $NaSO_4$ + 1 M methanol electrolytes. For comparison purposes, the photocurrent of a titanium foil (without anodization treatment) is also included although, showing a negligible photocurrent response. Photocurrent densities increase with the applied potential bias in all the electrodes and tend to reach a constant value at high potentials. As the magnitude of the anodic photocurrent is obviously proportional to the number of the photogenerated electrons transferred to the outer circuit, that means that the NTs prepared with higher applied potentials provide a more effective charge transport. In the absence of methanol, photocurrent is lower because only water photooxidation by photogenerated holes takes place at the electrode surface (see Fig. 2a and c). On the contrary, in presence of methanol, photocurrent increases due to methanol favours the diffusion length for photogenerated electrons, reduces recombination probability with surface-trapped holes [34,39] and/or actives the so-called current doubling effect [40]. The last mentioned reaction implies that the oxidation of methanol radical ($^{\bullet}CH_2OH$) to formaldehyde can take place directly at the electrode surface leading to an additional free electron at the anode that increases photocurrent density. This phenomenon has been observed in the photoelectrocatalytic oxidation for other organic molecules such as oxalate, formate, acetate or glucose [35,40,41].

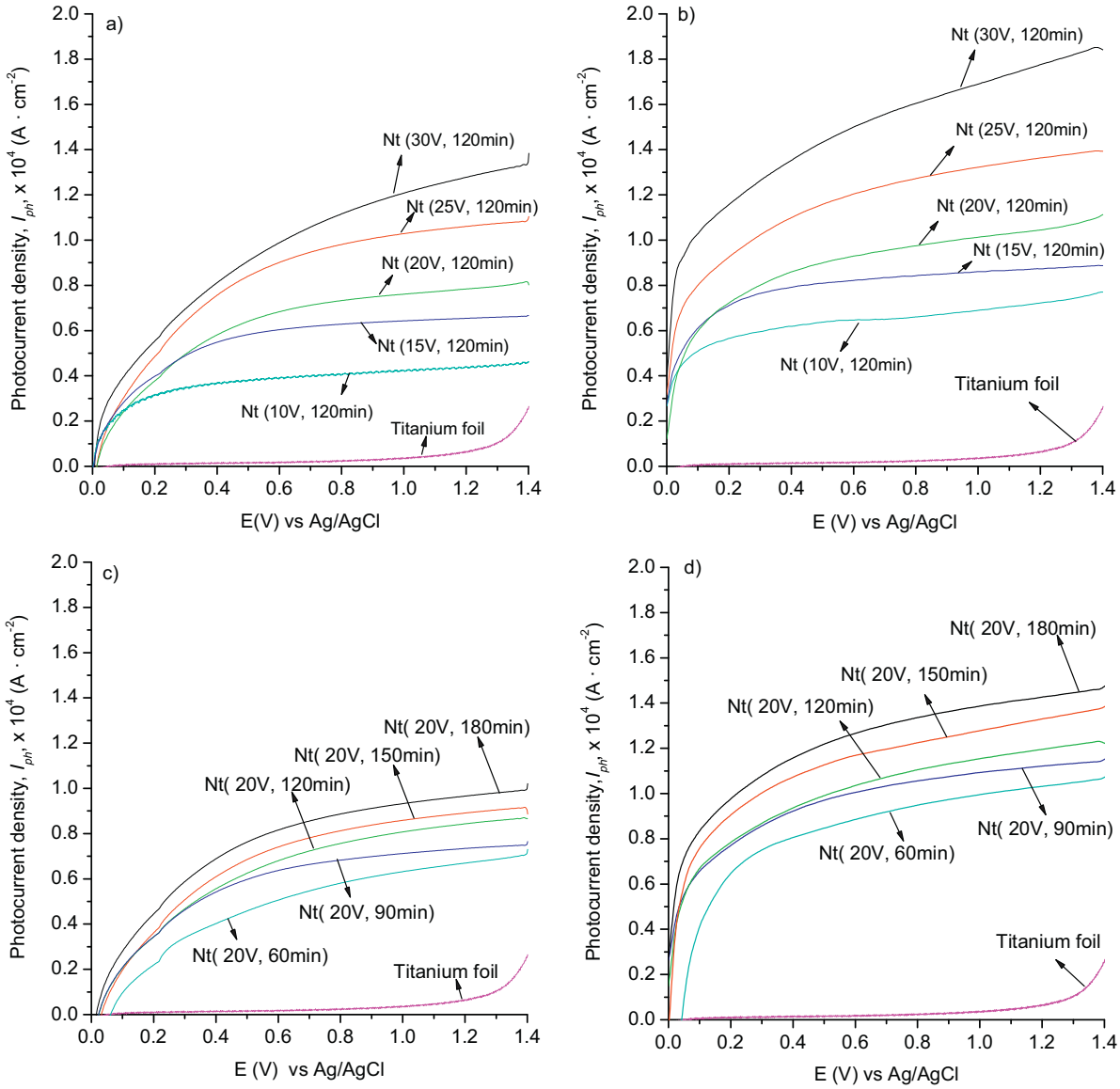

Fig. 2. Anodic branch from the cyclic photovoltammograms (CV) recorded at a sweep rate of 50 mV s^{-1} for the photoelectrodes anodized at 20 V and different anodization times in an electrolyte of a) 0.1 M Na_2SO_4 and b) 0.1 M Na_2SO_4 + 1 M of methanol; and for the photoelectrodes anodized at 120 minutes and different anodization potentials in an electrolyte of c) 0.1 M Na_2SO_4 and d) 0.1 M Na_2SO_4 + 1 M of methanol.

The increase in the photocurrent densities observed in Fig. 2 for both series of electrodes shows a clear correlation with the increasing thickness layer achieved for high anodization potential and time. This effect can be certainly explained by the increase in the amount of TiO_2 material available for absorbing the UV radiation provided by the light source.

This effect is clearly represented in Fig. 3 where a good linear correlation is observed between the nanotube length and the photocurrent density of both series of electrodes achieved at 1 V. All the data can be rather well fitted by a linear equation whose slope increases from 0.35 A cm^{-2} μm^{-1} to 0.5 A cm^{-2} μm^{-1} when 1 M of methanol is added to the electrolyte solution. This trend has been also studied and confirmed by other authors. For example, Hitchman et al. [42]. explain how the thickness of a thin film semiconductor is an important parameter in determining organic destruction efficiency, particularly when the light has to penetrate the particulate film before reaching the catalytic surface. The incident light has a maximum penetration depth into TiO_2 of $1/\alpha$, where α is the absorption coefficient of the TiO_2 at the wavelength of the incident light. The value of α for these photoanodes have been calculated from the UV–vis absorption spectra. The plot of the absorptivity of all the electrodes at 365 nm versus the length of the nanotubes in centimetres can be successfully fitted by a straight line with slope of $\alpha = 2.1 \times 10^3$ cm^{-1}. Therefore, an approximated estimation of the maximum penetration depth points out that the 90% of the irradiation can be absorbed in a range of 4.8 μm. This value is in agreement with other reports where photocatalytic efficiency increases with increasing NTs length, and then reaches a saturated value when the nanotubes are longer than 5 μm [43]. All the anodized electrodes shown in the present work have displayed layer thicknesses lower than the estimated maximum penetration depth hence it is concluded that radiation is not completely absorbed by the TiO_2-NTs layer and therefore the longer the nanotubes the higher light absorption. This fact explains the linear dependency shown in Fig. 3 with no signs of saturation. However, it is not expected that this trend continues increasing as the lengths of the NTs grow. For longer TiO_2-NTs than 4.8 μm the light begins to be not efficiently absorbed throughout the bulk and the photocurrent density versus NT length should reach a maximum. In any case, the intensity of the anodic photocurrent can be considered as a measure of the overall photoelectrocatalytic performance of an electrode which is determined by a serial of characteristic inherent to the material as adsorption capacity, surface morphology, crystal size, substrate-catalyst contact and the layer structure among them [41,44]. Hence the absolute photocurrent density values give an idea of the potential photocatalytic activity of these TiO_2-NTs photoanodes.

3.3. Photocatalytic and photoelectrocatalytic activity

Based on the photocurrent response of the studied photoanodes, selected TiO_2-NTs electrodes anodized at 20, 25 and 30 V during 120 min were scaled-up to circular supports 5 cm in diameter with an increased exposed area of 19.64 cm^2. This size is high enough to determine their photocatalytic (PC) and photoelectrocatalytic (PEC) activity under a fixed potential bias of 1 V and 1.4 V versus Ag/AgCl reference electrode. Activity values were evaluated by monitoring the formation of formaldehyde from methanol photooxidation using different initial methanol concentrations in a 0.1 M Na_2SO_4 electrolyte. The plot of formaldehyde concentration versus illumination time (not shown) represents a straight line that can be adjusted to a zero-order kinetic equation to obtain the rate constant k from the slope following a well-established procedure [34,45]. The blank experiment (electrode of titanium without TiO_2-NTs) reveals that the non-photocatalytic degradation of methanol is negligible (not shown). Fig. 4 shows the comparison between PC and PEC efficiencies in terms of kinetic constants for formaldehyde production (k) versus TiO_2-NTs length achieved for different initial methanol concentrations. As expected, the PC and PEC kinetic constants are higher as the TiO_2 layer thickness of the electrodes (NTs length) increases, in agreement with the photocurrent density values registered for these photoelectrodes (see Fig. 3). In general, higher values of k are also observed when increasing the initial concentration of methanol. PC kinetic constants of the NT25V and NT30V electrodes increase as methanol concentration is added to the solution confirming that methanol reduces recombination probability trapping the photogenerated surface holes [34,39]. On the contrary, PC k values for the NT20V photoanode remain constant independently of the initial methanol concentration.

A possible explanation of this behaviour is that when light irradiates the electrode, charge carriers are photogenerated in the TiO_2 layer that have to be rapidly transferred to the solution species before recombination. The amount of holes and electrons available is obviously related to the light absorbed by the TiO_2-NTs. In the case of NT20 V anode, displays a thickness of around 2 μm, and hence absorbs less amount of light than the other two electrodes and consequently generates lower amount of charge carriers. Therefore, less methanol molecules will be necessary to trap the available holes at the surface of the electrode, reaching saturation

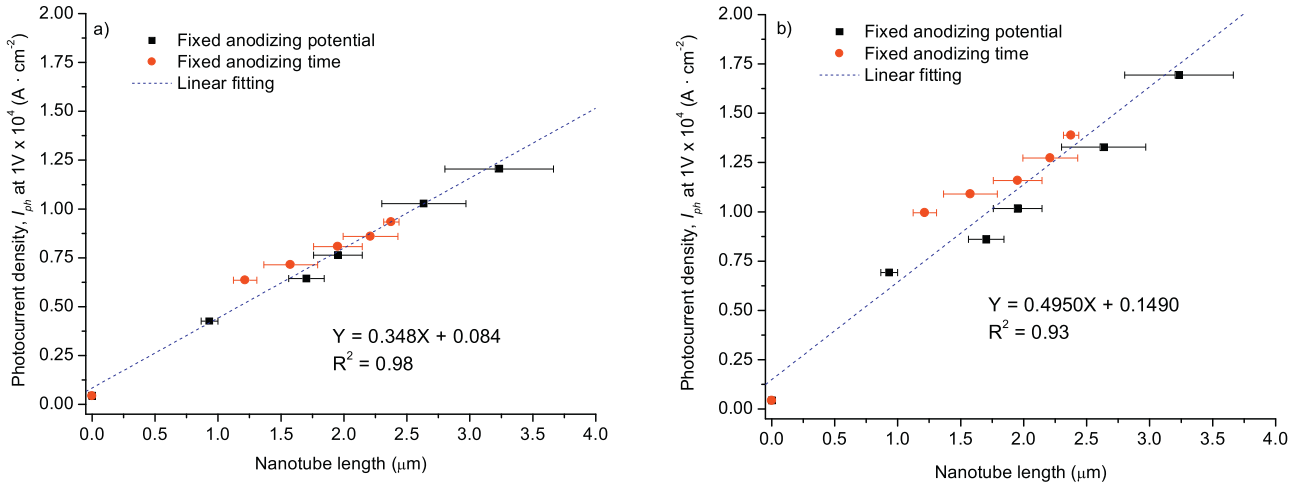

Fig. 3. Photocurrent density at 1 V vs NTs length for all the photoanodes in a) 0.1 M Na_2SO_4 electrolyte and b) 0.1 M Na_2SO_4 + 1 M of methanol electrolyte.

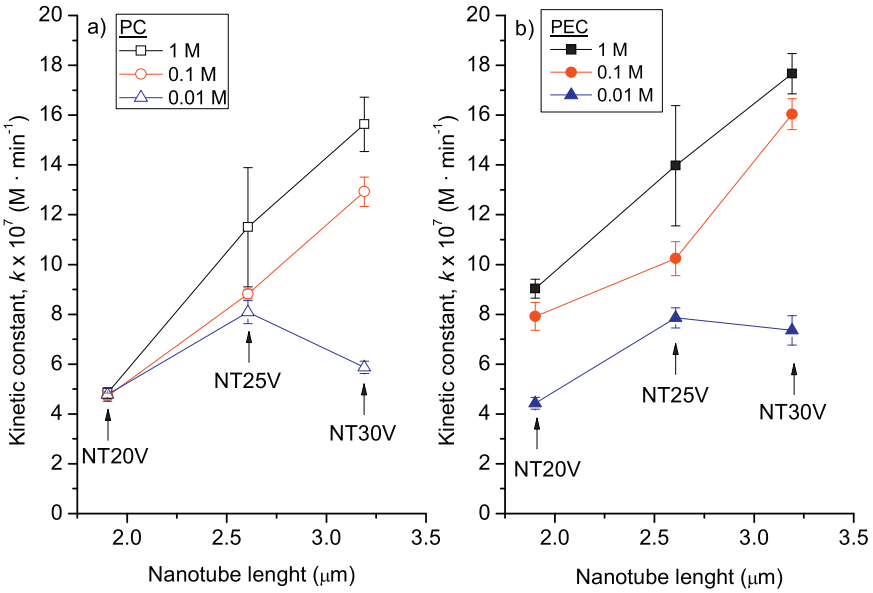

Fig. 4. Comparison of formaldahyde prodution kinetic constants at different initial concentrations of methanol of 1, 0.1 and 0.01 M with a) photocatalysis (PC) and b) photoelectrocatalysis (PEC). at 1 V of potential bias.

for lower methanol concentrations. This means that NT20 V electrode has either a poorer charge carrier transfer or, more likely, a lower light absorption capacity, being values of k not affected by methanol concentrations. On the other hand, due to charge balance, in steady state, the rate of oxidation by holes must be equal to the rate of reduction by electrons. Conversely, if the electrode generates higher amount of charges carriers and methanol concentration is not enough to trap the entire surface holes, the charges accumulate and the PC efficiency will decreases as a consequence of the recombination process. Although quantitative assessment of this hypothesis would require additional characterization data of the photoanodes based on impedance spectroscopy, this phenomenon is qualitatively observed in the PC experiments of NT25V and NT30V anodes at 0.01 M methanol concentration. Higher concentration of methanol gives rise to higher k values by reducing the recombination process and promoting charge transfer.

On the other hand, PEC experiments of Fig. 4 show that the application of a potential bias improves the reaction rate with all the tested TiO_2-NTs photoanodes. In this case, the photogenerated charges are subjected to an electric field opposed to their attraction forces. The electrons will be transferred to the metallic support, and conducted by the external circuit to the reduction reaction in the cathode, while the holes move to the surface of the TiO_2 photoanode to capture electrons from a donor through a oxidation reaction [34,42]. It is remarkable that when applying an anodic bias potential of 1 V to the NT20 V anode, the k values increases with methanol concentration. The calculated ratio between the k values of the PEC and the k of the PC experiments (k_{PEC}/k_{PC}) is in this electrode equivalent to 1.9, 1.6 and 1.0 when methanol concentration goes from 1 to 0.01 M. On the contrary, for the NT25 V and NT30 V electrodes the (k_{PEC}/k_{PC}) ratio only reaches a value between 1.3–1.0 times higher. Therefore, the electrode with shorter NTs length (NT20 V) is inhibiting in a better manner the recombination of the photogenerated electron–hole pairs when a bias potential is

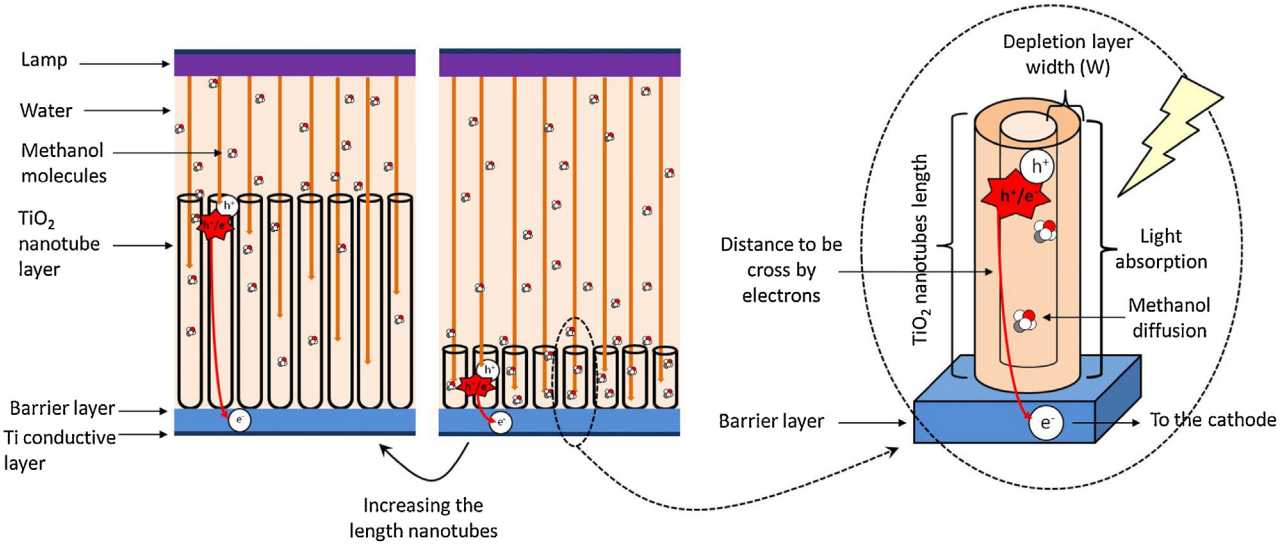

Fig. 5. Schematic representation of the suggested effect of the charges transport through a TiO_2-particulate film and through a TiO_2-NT layer.

applied. Indeed, it is well known that shorter NTs seem to favor the electron transport between TiO_2-NTs layer and the metallic conductive support which could be the main reason for this behavior [17]. This anode enhances almost 2-fold the *k* value of the PC at high methanol concentrations. As the nanotubes grow the *k* values of both reactions (PC and PEC) tend to be similar and the charge separation effect decreases (see NT25V and NT30V electrodes).

The mechanism that involves the formation and motion of the charge carriers within a TiO_2 layer is a complex processes that depends on various phenomena that can be defined mainly as the balance between the light absorption by the TiO_2 and the photogenerated charges diffusion. In Fig. 5 is shown a schematic draw of the phenomena that control this process.

For generated electrons this diffusion should be through the TiO_2 layer and towards the positive current collector (cathode) and for the holes the diffusion goes to the depletion layer width (W) to the surface [41,42]. Holes generated at a distance from the surface lower than W will be efficiently transported to the surface, whereas holes generated deeper between W and (W + Lp), where Lp is the minority carrier length, may diffuse to the depletion layer boundary and be transported to the surface or may recombine with electrons. The recombination is the most likely process for charges generated at depths higher than (W + Lp) [41,46]. In TiO_2, the minority carrier length (Lp) is the maximum distance that the holes can move in a field-free region before getting recombine with an electron. This distance has been estimated in about 0.1 μm [46]. Therefore, although light absorption (and charge generation) is favoured in thicker TiO_2 layers, the thickness of TiO_2 layer (NTs length) also has a strong influence in the electron diffusion. As the distance to be crossed by electrons up to reaching the conductive support increases, their changes of being lost by recombination through the TiO_2 layer also increases [17]. This is in agreement with the report of Liu et al [43] about the simulation of the photocatalytic efficiency on different NTs morphological parameters for different O_2 diffusion coefficients. These authors have observed that photocatalytic efficiency firstly increases and then decreases as the inner diameter and wall thickness of the nanotubes increase. The oxygen transport within the TiO_2 nanotubes increases as these parameters increase, which will improve photocatalytic activity. On the other hand, photocatalytic efficiency increases as NTs length increases, and tends to reach a saturation plateau, which is mainly influenced by the change of light absorption and the diffusion of reactants along the NTs. The latter can be explained considering that as nanotubes get longer, the migration of reactant/products along the tube becomes hindered and the accumulation of the products restrains the surface reaction of holes (see Fig. 5). This effect can be partially counteracted by the improvement in diffusion provided by wider tube channels, which indicates that the inner diameter may play a significant role in the PEC activities of TiO_2 nanotubes [47].

Interestingly, Liu et al. [24] present other point of view. These authors have found that the activity dependence on the nanotube length in the PEC process is exactly opposite to the PC process. In the PC degradation of phenol by nanotube arrays, the increased length improves the activity greatly until reaching saturation because the nanotube length favors the light absorption and the saturated PC activity can be explained by considering the saturated light trapping and the limited diffusion distance of the phenol solution into the nanotube arrays. However, our results point out that the PEC process also tends to reach a saturation plateau. This is due to in the PEC process although the increased length of the nanotube arrays will generate more photogenerated charges by the UV light, this also will increase the resistance of the TiO_2 nanotube array and the photogenerated electrons will track a long distance through the TiO_2 nanotube to reach the metallic support [35]. This fact will increase the probability of the charge recombination.

Fig. 6a shows the influence of increasing the electric potential bias applied on the values of the kinetic constant (*k*) of methanol photoxidation, whereas Fig. 6b shows the dependence of the k_{PEC}/k_{PC} on the nanotube length. In all cases, the application of a potential bias of 1 V increases the efficiency of TiO_2-NTs photoelectrodes, being the improvement in the efficiency even higher when 1.4 V is applied. This dependence on the applied potential indicates that the depletion layer is completely developed and that electron transport is still the controlling step of the overall process for high electric potential bias, which means that charge carrier separation takes place for the whole range of applied electric potential bias [34]. It must be noticed that although the NT20 V electrode shows better properties for charge carrier separation in comparison with the NT25 V and NT30 V electrodes, the values of *k* for NT20 V electrode are much lower compared to the other two

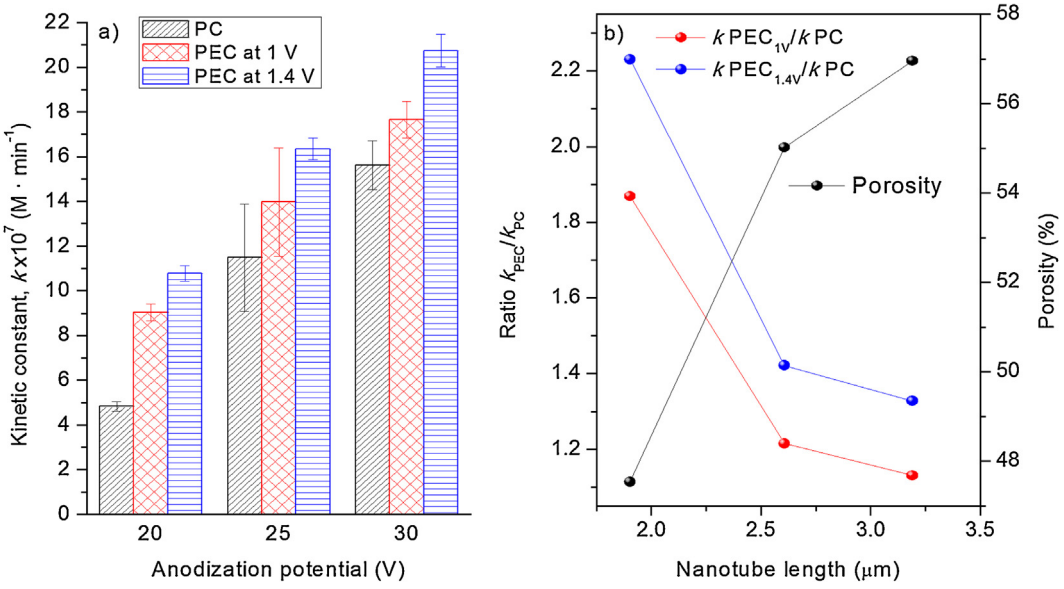

Fig. 6. a) Influence of the electric potential bias applied (PC, +1.0, and +1.4 V) on the values of the surface zero-order kinetic constant (k) for formaldehyde production due to methanol oxidation b) Representation of the k_{PEC}/k_{PC} ratio at 1 and 1.4 V and porosity versus nanotube length.

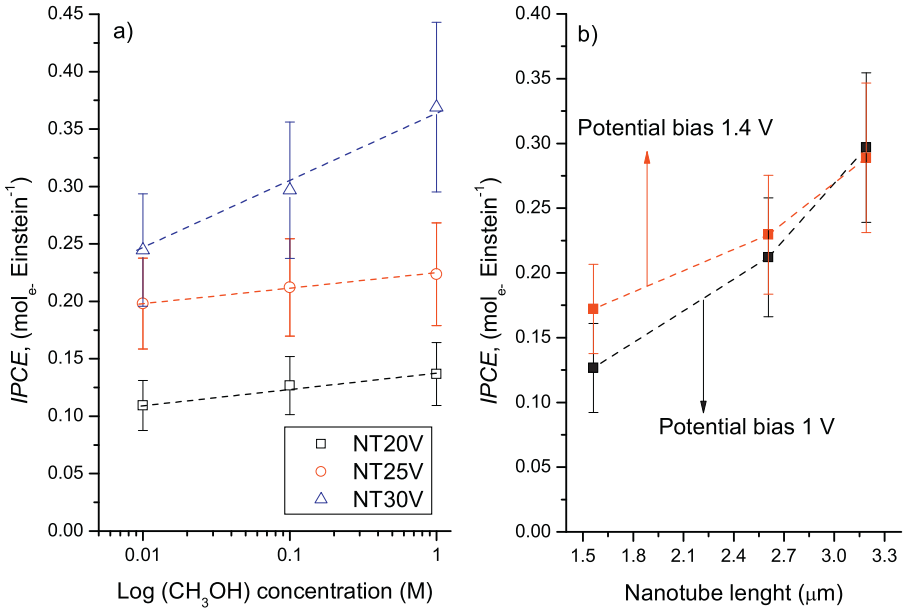

Fig. 7. Incident photon-to-current efficiencies during the photoelectrocatalytic (PEC) experiments for a) the three electrodes in different methanol concentrations (0.01, 0.1 and 1 M) at 1 V and for b) the three electrodes in a 0.1 M Na_2SO_4 + 1 M of methanol electrolyte at 1 and 1.4 V.

electrodes. In contrast, NT25 V and NT30 V electrodes seem to show suitable properties for favoring charge carrier transfer on their TiO_2 surface since they present a high surface in contact with the electrolyte leading to a higher photocatalytic activity. Fig. 6b also shows the values estimated for porosity (Table 1S), showing a trend with the nanotube length opposite to the k_{PEC}/k_{PC} ratio. These results contrast with those provided by the study of Liang et al. [47]. who found that photoconversion efficiency for water splitting of TiO_2 nanotube arrays increases exponentially when the porosity increases. A possible explanation for this discrepancy could be related to the external diffusion of the electron donors in the nanotubes, strongly condition by their diameter and whose effect could be completely different depending on the studied reaction.

Finally, Fig. 7 shows the effect of initial methanol concentration and nanotubes length on the incident photon-to-current efficiency (IPCE). IPCE is a measurement of the photoelectrochemical efficiency defined as the ratio between the amount of electrons generated on the external circuit (calculated in $mol_{e^-}\,s^{-1}\,cm^{-2}$ by dividing the current density in $A\,cm^{-2}$ by the Faraday constant, $F = 96485\ A\,s{\cdot}mol_{e^-}{}^{-1}$) and the amount of photons incident to the system (calculated in $Einstein\,s^{-1}\,cm^{-2}$ by dividing the radiation flux in $W\,cm^{-2}$ by the molar energy of photons of 365 nm in wavelength, $h\nu$) [33]. In all cases a linear trend is observed, with higher IPCE: i as the NTs-TiO_2 layer thickness increases, due to improved radiation absorption; and, ii a higher methanol concentration, due to an improved charge transfer. However, IPCE tends to reach a maximum with NTs of 3.2 μm even when higher potential bias is applied. This fact demonstrates that charge separation is the limiting step due to the fact that the resistance of the TiO_2 nanotube arrays to the electrons conduction, increases with nanotubes longer thicknesses. Interestingly, these effects are even more pronounced that they were observed in the values of the kinetics constants (Figs. 4 b and 6 a). As the NTs-TiO_2 layer thickness increases, the methanol concentration becomes a more important factor due to the increased effect of trapping holes at higher surface areas. On the other hand, NT20V is more influenced by the applied potential bias due to the favoured charge recombination in its short nanotubes. However, in comparison with particulate electrodes, the intimate contact of the nanotubes with the support and the absence of grain boundaries make the electron transport much more efficient [33,34]. These results show that the highly ordered nanotube arrays make possible the directly correlation between photocurrent density and photoelectrocatalytic activity.

4. CONCLUSIONS

Physicochemical and photoelectrochemical characterization of highly ordered TiO_2 nanotube array photoanodes has shown a good correlation with their activity in photocatalytic and photoelectrocatalytic reactions. An increase in the length of the nanotubes leads to a significant increase both in the photocatalytic and photoelectrocatalytic measured reaction rates due to the increased surface area. Although thicker TiO_2 layers (longer NTs) also enhances light absorption, a compromise must be reached, as the longer diffusion distance for the electrons to reach the back contact of the electrode increases transport resistance. This effect is confirmed by the reduction in the enhancement of the activity of the PEC reaction in comparison with the PC process, confirming that the improvement effect of the charge separation is progressively lost. The main conclusion is that the length of the TiO_2-NTs should be finely tuned to optimize the compromise between light absorption reactivity and transport properties to maximize the reaction rate.

ACKNOWLEDGEMENTS

The authors gratefully acknowledge the financial support of the European Commission under FP7 project 309846, “Photocatalytic Materials for the Destruction of Recalcitrant Organic Industrial Waste – PCATDES”. This work has been also partially financed through the project funded by Spanish Ministry of Economy and Competitiveness (MINECO), in the frame of the collaborative international consortium WATERJPI2013 – MOTREM of the Water Challenges for a Changing World Joint Programming Initiative (Water JPI) Pilot Call and Comunidad de Madrid through the program REMTAVARES (S2013/MAE-2716). Help of Dr. Gilberto del Rosario with the interpretation and analysis of the FEG-SEM images is also acknowledged.

Appendix A. Supplementary data

Supplementary data associated with this article can be found, in the online version, at http://dx.doi.org/10.1016/j.electacta.2016.01.088.

References

[1] N. Liu, X. Chen, J. Zhang, J.W. Schwank, A review on TiO_2-based nanotubes synthesized via hydrothermal method: Formation mechanism, structure modification, and photocatalytic applications, Catalysis Today 225 (2014) 34–51.

[2] P. Roy, S. Berger, P. Schmuki, TiO_2 nanotubes: Synthesis and applications, Angew. Chem. Int. Ed 50 (2011) 2904–2939.

[3] S.K. Mohapatra, M. Misra, V.K. Mahajan, K.S. Raja, Design of a highly efficient photoelectrolytic cell for hydrogen generation by water splitting: application of $TiO_{2-x}C_x$ nanotubes as a photoanode and Pt/TiO_2 nanotubes as a cathode, J. Phys. Chem. 11 (2007) 8677–8685.

[4] G.F. Ortiz, I. Hanzu, T. Djenizian, P. Lavela, J.L. Tirado, P. Knauth, Alternative Li-ion battery electrode based on self-organized titania nanotubes, Chem. Mater. 21 (2009) 63–67.

[5] G.K. Mor, O.K. Varghese, M. Paulose, K.G. Ong, C.A. Grimes, Fabrication of hydrogen sensors with transparent titanium oxide nanotube-array thin films as sensing elements, Thin Sol. Films 496 (2006) 42–48.

[6] A. Ghicov, S.P. Albu, R. Hahn, D. Kim, T. Stergiopoulos, J. Kunze, C.A. Schiller, P. Falaras, P. Schmuki, TiO_2 nanotubes in dye-sensitized solar cells: Critical factors for the conversion efficiency, Chem. Asian J. 4 (2009) 520–525.

[7] S. Yoriya, N. Bao, C.A. Grimes, Titania nanoporous/tubular structures via electrochemical anodization of titanium: effect of electrolyte conductivity and anodization voltage on structural order and porosity, J. Mater. Chem. 21 (2011) 13909–13912.

[8] C.J. Lin, W.Y. Yu, Y.T. Lu, S.H. Chien, Fabrication of open-ended high aspect-ratio anodic TiO_2 nanotube films for photocatalytic and photoelectrocatalytic applications, Chem. Comm. 45 (2008) 6031–6033.

[9] K. Shankar, J.I. Basham, N.K. Allam, O.K. Varghese, Mor G.K, X. Feng, M. Paulose, J.A. Seabold, K.-Shin Choi, C.A. Grimes, Recent advances in the use of TiO_2 nanotube and nanowire arrays for oxidative photoelectrochemistry, J. Phys. Chem. C 113 (2009) 6327–6359.

[10] M.D. García Rodríguez, B. Sánchez, J.M. Coronado, Revisiting the hydrothermal synthesis of titanate nanotubes: new insights on the key factors affecting the morphology, Nanoscale 3 (2011) 2233–2240.

[11] T. Zhao, Z. Liu, K. Nakata, S. Nishimoto, T. Murakami, Y. Zhao, L. Jiang, A. Fujishima, Multichannel TiO_2 hollow fibers with enhanced photocatalytic activity, J. Mater. Chem. 20 (2010) 5095–5099.

[12] T. Kasuga, M. Hiramatsu, A. Hoson, T. Sekino, K. Niihara, Formation of Titanium Oxide Nanotube, Langmuir 14 (1998) 3160–3163.

[13] V. Zwilling, E. Darque-Ceretti, A. Boutry-Forveille, D. David, M.Y. Perrin, M. Aucouturier, Structure and physicochemistry of anodic oxide films on titanium and TA6 V alloy, Surf. Interface Anal. 27 (1999) 629–637.

[14] H.E. Prakasam, K. Shankar, M. Paulose, O.K. Varghese, C.A. Grimes, A new benchmark for TiO_2 nanotube array growth by anodization: A new benchmark for TiO_2 nanotube array growth by anodization, J. Phys. Chem. C 111 (2007) 7235–7241.

[15] R. Beranek, H. Hildebrand, P. Schmuki, Self-organized porous titanium oxide prepared in H_2SO_4/HF electrolytes Electrochem, Solid State Lett. 6 (2003) B12–B14.

[16] K. Rajeshwar, M.E. Osugi, W. Chanmanee, C.R. Chenthamarakshan, M.V.B. Zanoni, P. Kajitvichyanukul, R. Krishnan-Ayer, Heterogeneous photocatalytic treatment of organic dyes in air and aqueous media: J, Photochem. Photobiol. C: Photochem. Rev. 9 (2008) 171–192.

[17] V. Likodimos, T. Stergiopoulos, P. Falaras, J. Kunze, P. Schmuki, Phase composition, size, orientation, and antenna effects of self-assembled anodized titania nanotube arrays: A polarized micro-Raman investigation, J. Phys. Chem. C 112 (2008) 12687–12696.

[18] Y. Alivov, M. Pandikunta, S. Nikishin, Z.Y. Fan, The anodization voltage influence on the properties of TiO_2 nanotubes grown by electrochemical oxidation, Nanothecnology 20 (2009) 225602–225608.

[19] D. Gong, C.A. Grimes, O.K. Varghese, W. Hu, R.S. Singh, Z. Chen, E.C. Dickey, Titanium oxide nanotube arrays prepared by anodic oxidation, J. Mater. Res. 16 (2001) 3331–3334.

[20] F.R. Cummings, L.J. Le Roux, M.K. Mathe, D. Knoesen, Structure induced optical properties of anodized TiO_2 nanotubes, Mater. Chem. Phys. 124 (2010) 234–242.

[21] J.M. Macak, H. Tsuchiya, A. Ghicov, K. Yasuda, R. Hahn, S. Bauer, P. Schmuki, TiO_2 nanotubes: Self-organized electrochemical formation, properties and applications, Curr. Opin. Solid State Mater. Sci. 11 (2007) 3–18.

[22] D. Regonini, A. Satka, A. Jaroenworaluck, D.W.E. Allsopp, C.R. Bowen, R. Stevens, Factors influencing surface morphology of anodized TiO_2 nanotubes, Electrochim. Acta 74 (2012) 244–253.

[23] G.K. Mor, O.K. Varghese, P. Maggie, N. Mukherjee, C.A. Grimes, Fabrication of tapered, conical-shaped titania nanotubes, J. Mater. Res. 18 (2003) 2588–2593.

[24] Z. Liu, X. Zhang, S. Nishimoto, M. Jin, D.A. Tryk, T. Murakami, A. Fujishima, Highly ordered TiO_2 nanotube arrays with controllable length for photoelectrocatalytic degradation of phenol, J. Phys. Chem. C 112 (2008) 253–259.

[25] V.C. Anitha, D. Menon, S.V. Nair, R. Prasanth, Electrochemical tuning of titania nanotube morphology in inhibitor electrolytes, Electrochim. Acta 55 (2010) 3703–3713.

[26] J.M. Macak, Patrik Schmuki, Anodic growth of self-organized anodic TiO_2 nanotubes in viscous electrolytes, Electrochim. Acta 52 (2006) 1258–1264.

[27] Q. Cai, M. Paulose, O.K. Varghese, C.A. Grimes, The effect of electrolyte composition on the fabrication of self-organized titanium oxide nanotube arrays by anodic oxidation, J. Mater. Res. 20 (2005) 230–236.

[28] D. Fang, Z. Luo, K. Huang, D.C. Lagoudas, Effect of heat treatment on morphology, crystalline structure and photocatalysis properties of TiO_2 nanotubes on Ti substrate and freestanding membrane, Appl. Surf. Sci. 257 (2011) 6451–6461.

[29] W. Chanmanee, A. Watcharenwong, C. Chenthamarakshan, P. Kajitvichyanukul, N.R. de Tacconi, K. Rajeshwar, Formation and characterization of self-organized TiO_2 nanotube arrays by pulse anodization, J. Am. Chem. Soc. 130 (2008) 965–974.

[30] G.K. Mor, K. Shankar, M. Paulose, O.K.C.A. Varghese, Grimes,Enhanced photocleavage of water using titania nanotube arrays, Nano Lett. 6 (2006) 215–218.

[31] H.-F. Zhuang, C.-J. Lin, Y.-K. Lai, L. Sun, J. Li, Some critical structure factors of titanium oxide nanotube array in its photocatalytic activity, Environ. Sci. Technol. 41 (2007) 4735–4740.

[32] D.A. Tryk, A. Fujishima, K. Honda, Recent topics in photoelectrochemistry: achievements and future prospects, Electrochim. Acta 45 (2000) 2363–2376.

[33] J. Marugán, R. van Grieken, C. Pablos, C. Adán, R. Timmers, Determination of photochemical, electrochemical and photoelectrochemical efficiencies in a photoelectrocatalytic reactor, Int. J. Chem. React. Eng. 0 (2013) 1–11.

[34] C. Pablos, J. Marugán, R. van Grieken, C. Adán, A. Riquelme, J. Palma, Correlation between photoelectrochemical behaviour and photoelectrocatalytic activity and scaling-up of P25-TiO_2 electrodes, Electrochim. Acta 130 (2014) 261–270.

[35] D. Jiang, H. Zhao, S. Zhang, R. John, Characterization of photoelectrocatalytic processes at nanoporous TiO_2 film electrodes: Photocatalytic oxidation of glucose, J. Phys. Chem. B 107 (2003) 12774–12780.

[36] M.A. Butler, Photoelectrolysis and physical properties of the semiconducting electrode WO_2, J. Appl. Phys. 48 (1977) 1914–1920.

[37] A.G. Kontos, A. Katsanaki, T. Maggos, V. Likodimos, A. Ghico, D. Kim, J. Kunze, C. Vasilakos, P. Schmuki, P. Falaras, Photocatalytic degradation of gas pollutants on self-assembled titania nanotubes, Chem. Phys. Lett. 490 (2010) 58–62.

[38] T. Nash, The colorimetric estimation of formaldehyde by means of Hantzsch reaction, J. Biochem. 55 (1953) 416–421.

[39] R.P. Lynch, A. Ghicov, P. Schmuki, A photo-electrochemical investigation of self-organized TiO_2 nanotubes, J. Electrochem. Soc. 157 (2010) G76–G84.

[40] J.A. Byrne, B.R. Eggins, S. Linquette-Mailley, P.S. Dunlop, The effect of hole acceptors on the photocurrent response of particulate TiO_2 anodes, Analyst 123 (1998) 2007–2012.

[41] M. Uzunova, M. Kostadinov, J. Georgieva, C. Dushkin, D. Todorovsky, N. Philip-Pidis, I. Poulios, S. Sotiropoulos, Photoelectrochemical characterisation and photocatalytic activity of composite La_2O_3–TiO_2 coatings on stainless steel, Appl. Catal. B: Environ. 73 (2007) 23–33.

[42] M.L. Hitchman, F. Tian, Studies of TiO_2 thin films prepared by chemical vapour deposition for photocatalytic and photoelectrocatalytic degradation of 4-chlorophenol, J. Electroanal. Chem. 538-539 (2002) 165–172.

[43] B. Liu, K. Nakata, S. Liu, M. Sakai, T. Ochiai, T. Murakami, K. Takagi, A. Fujishima, Theoretical kinetic analysis of heterogeneous photocatalysis by TiO_2 nanotube arrays: the effects of nanotube geometry on photocatalytic activity, J. Phys. Chem. C 116 (2012) 7471–7479.

[44] F. Cao, G. Oskam, G.J. Meyer, P.C. Searson, Electron transport in porous nanocrystalline TiO_2 photoelectrochemical cells, J. Phys. Chem. 100 (1996) 17021–17027.

[45] J. Marugán, D. Hufschmidt, M.J. López-Muñoz, V. Selzer, D. Bahnemann, Photonic efficiency for methanol photooxidation and hydroxyl radical generation on silica-supported TiO_2 photocatalysts, Appl. Catal. B: Environ. (2006) 201–207.

[46] I.M. Butterfield, P.A. Christensen, A. Hamnett, K.E. Shaw, G.M. Walker, S.A. Walker, C.R. Howarth, Applied studies on immobilized titanium dioxide films as catalysts for the photoelectrochemical detoxification of water, J. Appl. Electrochem. 27 (1997) 385–395.

[47] S. Liang, J. He, Z. Sun, Q. Liu, Y. Jiang, H. Cheng, B. He, Z. Xie, S. Wei, Improving photoelectrochemical water splitting activity of TiO_2 nanotube arrays by tuning geometrical parameters, J. Phys. Chem. C 116 (2012) 9049–9053.